Aalborg Universitet

A SAGE Algorithm for Estimation of the Direction Power Spectrum of Individual Path Components

Xuefeng Yin*, Lingfeng Liu*, Daniel K. Nielsen*, Troels Pedersen* and Bernard H. Fleury*‡

*Section Navigation and Communications, Department of Electronics Systems,
Aalborg University, DK-9220 Aalborg, Denmark
‡Forschungszentrum Telekommunikation Wien (ftw.), Vienna, Austria
Email: {xuefeng,lingfeng,dkni02,troels,bfl}@es.aau.dk

Abstract—In this contribution, the Fisher-Bingham-5 (FB5) probability density function (pdf) is used to model the shape of the direction power spectral density function (psdf) of individual path components in the radio channel. The FB5 distribution is selected because, among all direction distributions, it maximizes the entropy under the constraints that the first and second distribution moments are specified. A SAGE (Space-Alternating Generalized Expectation-maximization) algorithm is derived based on this model for estimation of the parameters characterizing the direction psdf of each path component in a multi-path scenario. The performance of the SAGE algorithm is evaluated using measurement data. Preliminary results show that the estimated direction psdfs of individual path components exhibit different ovalnesses and tilt angles. These density functions are noticeably more concentrated than the corresponding footprints in the Bartlett spectrum.

Index Terms—Terms-Path component, Fisher-Bingham-5, direction dispersion, radio channel, SAGE algorithm

I. INTRODUCTION

Due to the heterogeneity of the propagation environment, the response of the radio channel can be viewed as the superposition of a certain number of components. Each component, which we refer to as "path component", is contributed by an electromagnetic wave propagating along a path from the transmitter (Tx) to the receiver (Rx). Along this path, the wave interacts with a certain number of objects called scatterers. Due to the geometrical extent and the nonhomogeneous electromagnetic properties of the scatterers, a path may be dispersive in delay, direction of departure, direction of arrival, polarizations, as well as in Doppler frequency when the environment is time-variant. As a consequence, an individual path component may be spread in these dispersion dimensions. Modeling of these dispersion phenomena is required for the design and optimization of mobile communication systems and thus, experimental knowledge of the dispersive characteristics of path components is necessary.

In recent years, estimation of the dispersive characteristics of individual path components in multiple dimensions has attracted much attention. Some of the techniques are derived using the assumption that the normalized power spectral density function (psdf) of individual path components can be described using a certain probability density function (pdf). In [1], the product of the von-Mises pdf and the exponential pdf is used to model the normalized delay–Azimuth-of-Arrival (AoA) psdf.

In [2] and [3], the von–Mises–Fisher and Fisher–Bingham–5 (FB5) pdfs are used to characterize the normalized AoA–Azimuth-of-Departure (AoD) psdf and direction (azimuth and elevation) psdf respectively. The normalized delay–AoA–AoD psdf is characterized using a 3-variate pdf derived in [4].

In this contribution, we derive a SAGE algorithm to estimate the direction (azimuth and elevation) power spectrum of individual path components. The normalized direction psdf is modeled using the FB5 pdf as described in [3]. The SAGE algorithm is applied to measurement data to estimate the direction power spectra of multiple dispersive path components.

This contribution is organized as follows. In Section II, a signal model for channel sounding is presented and characterization of the normalized direction psdf using the FB5 pdf is introduced. In Section III, the estimators of the model parameters are derived within the SAGE framework. Section IV shows the experimental results. Finally concluding remarks are provided in Section V.

II. SIGNAL MODEL

In this contribution, we focus on the dispersive characteristics of individual path components in direction of arrival (DoA). The channel sounding system considered has a SIMO (single-input multiple-ouput) configuration with a single Tx antenna and a M-element Rx antenna array. The signal model, the characterization method, and the estimation method derived here can be easily modified to handle a MISO (multiple-input single-ouput) channel sounding configuration where dispersion in direction of departure (DoD) is of interest.

We consider narrow-band transmission, which implies that the product of the signal bandwidth times the channel delay spread is much smaller than one. Following the nomenclature in [5], the continuous-time output signal of the Rx array of the SIMO system reads

$$\boldsymbol{Y}(t) = \boldsymbol{H}(t)u(t) + \boldsymbol{W}(t) \in \mathbb{C}^M$$
$$= \left[\int_{\mathbb{S}_2} \boldsymbol{c}(\boldsymbol{\Omega}) h(t; \boldsymbol{\Omega}) \mathrm{d}\boldsymbol{\Omega} \right] u(t) + \boldsymbol{W}(t). \quad (1)$$

The complex vector $\boldsymbol{Y}(t)$ contains the output signals of the Rx array observed at time instance t. The scalar function $u(t)$ denotes the complex envelope of the transmitted sounding signal at time t. The vector $\boldsymbol{H}(t)$ represents the time-variant response of the SIMO system. We assume that $u(t)$

is known to the Rx and that $\int_0^T u(t)u(t)^* \mathrm{d}t = 1$, where $[\cdot]^*$ denotes complex conjugate and T represents the duration of observation interval. The function $h(t;\boldsymbol{\Omega})$ is the (time-variant) DoA spread function of the propagation channel [5]. Here, $\boldsymbol{\Omega}$ denotes the DoA, which is defined to be a unit vector with initial point anchored at the origin $\mathcal{O}$ of a coordinate system located in the vicinity of the Rx array. The end point of $\boldsymbol{\Omega}$ lies on a unit sphere $\mathbb{S}_2$ centered at $\mathcal{O}$. The DoA $\boldsymbol{\Omega}$ is uniquely determined by the spherical coordinates $(\phi, \theta) \in [-\pi, \pi) \times [0, \pi]$ of its end point according to the relation

$$\boldsymbol{\Omega} = \begin{bmatrix} \cos(\phi)\sin(\theta) \\ \sin(\phi)\sin(\theta) \\ \cos(\theta) \end{bmatrix}. \tag{2}$$

The angles ϕ and θ are referred to as the AoA and elevation of arrival (EoA) respectively. The noise $\boldsymbol{W}(t)$ in (1) is a vector-valued, circularly symmetric, spatially and temporally white Gaussian process with component spectral height σ_w^2. We assume that σ_w^2 can be measured and therefore is known in advance. In (1) the complex vector

$$\boldsymbol{c}(\boldsymbol{\Omega}) \doteq [c_1(\boldsymbol{\Omega}), c_2(\boldsymbol{\Omega}), \ldots, c_M(\boldsymbol{\Omega})]^{\mathrm{T}} \tag{3}$$

with $[\cdot]^{\mathrm{T}}$ denoting transposition is the responses of the Rx array. In a scenario where the electromagnetic energy propagates from the Tx to the Rx via D paths, the DoA spread function $h(t;\boldsymbol{\Omega})$ can be decomposed as

$$h(t;\boldsymbol{\Omega}) = \sum_{d=1}^{D} h_d(t;\boldsymbol{\Omega}). \tag{4}$$

The summand $h_d(t;\boldsymbol{\Omega})$ denotes the dth path component in $h(t;\boldsymbol{\Omega})$.

We assume that the transfer vector $\boldsymbol{H}(t)$ fluctuates over the overall sounding period, but remains constant within individual observation intervals:

$$\boldsymbol{H}(t) \doteq \boldsymbol{H}_n, \quad t \in [t_n, t_n + T) \text{ and } n \in [1, \ldots, N]. \tag{5}$$

Here, t_n denotes the time instance at which the nth observation interval starts and N represents the number of observation intervals. Similarly, the spread functions $h_d(t;\boldsymbol{\Omega})$, $d = 1, \ldots, D$ arising in (4) are constant within individual observation intervals:

$$h_d(t;\boldsymbol{\Omega}) = h_d(t_n;\boldsymbol{\Omega}) \doteq h_{d,n}(\boldsymbol{\Omega}), \quad t \in [t_n, t_n + T). \tag{6}$$

The processes $h_{d,n}(\boldsymbol{\Omega})$, $n \in [1, \ldots, N]$, $d \in [1, \ldots, D]$ are assumed to be uncorrelated complex (zero-mean) orthogonal stochastic measures, i.e.

$$\mathrm{E}[h_{d,n}^*(\boldsymbol{\Omega})h_{d',n'}(\boldsymbol{\Omega}')] = P_d(\boldsymbol{\Omega})\delta_{nn'}\delta_{dd'}\delta(\boldsymbol{\Omega} - \boldsymbol{\Omega}'). \tag{7}$$

Here, $\delta_{(\cdot)}$ and $\delta(\cdot)$ represent the Kronecker delta and the Dirac delta function respectively, and $P_d(\boldsymbol{\Omega}) \doteq \mathrm{E}[|h_{d,n}(\boldsymbol{\Omega})|^2]$ denotes the direction psdf of the dth path component. Identity (7) implies that the spread functions of distinct individual path components or at different observation intervals are

uncorrelated. This scenario is referred to as the *uncorrelated scattering* case in the literature (see e.g. [5]).

The direction psdf $P_d(\boldsymbol{\Omega})$ describes the manner the average power of the dth path component is distributed on the unit sphere $\mathbb{S}_2$. It can be written as

$$P_d(\boldsymbol{\Omega}) = P_d \cdot f_d(\boldsymbol{\Omega}) \tag{8}$$

with P_d representing the average power of the dth path component and $f_d(\boldsymbol{\Omega})$ being a normalized direction psdf.

In this contribution, we assume that $f_d(\boldsymbol{\Omega})$ coincides with the FB$_5$ pdf [6]. Among all distributions on the unit sphere $\mathbb{S}_2$, the FB$_5$ distribution [6] maximizes the entropy under the constraints that the distribution first and second moments are specified. The first moment of the distribution is parameterized by the nominal direction, while the second moments are characterized by parameters describing the concentration and the ovalness of the spreads of $f_d(\boldsymbol{\Omega})$ on $\mathbb{S}_2$. The pdf $f_{\mathrm{FB}_5}(\boldsymbol{\Omega})$ reads

$$f_{\mathrm{FB}_5}(\boldsymbol{\Omega}) = C(\kappa,\eta)^{-1} \exp\{\kappa\boldsymbol{\gamma}_1^{\mathrm{T}}\boldsymbol{\Omega} \\ + \kappa \cdot \eta[(\boldsymbol{\gamma}_2^{\mathrm{T}}\boldsymbol{\Omega})^2 - (\boldsymbol{\gamma}_3^{\mathrm{T}}\boldsymbol{\Omega})^2]\}, \tag{9}$$

where $\kappa \geq 0$ represents the concentration parameter and $\eta \in [0, 1/2)$ is an ovalness factor. In (9), $C(\kappa,\eta)$ denotes a normalization constant depending on κ and η, $\boldsymbol{\gamma}_1$, $\boldsymbol{\gamma}_2$, and $\boldsymbol{\gamma}_3 \in \mathbb{R}^3$ are unit vectors. The matrix $\boldsymbol{\Gamma} \doteq [\boldsymbol{\gamma}_1, \boldsymbol{\gamma}_2, \boldsymbol{\gamma}_3]$ is uniquely determined by three angular parameters $\bar{\theta}$, $\bar{\phi}$ and α according to

$$\boldsymbol{\Gamma} = \begin{bmatrix} \sin(\bar{\theta})\cos(\bar{\phi}) & -\sin(\bar{\phi}) & \cos(\bar{\theta})\cos(\bar{\phi}) \\ \sin(\bar{\theta})\sin(\bar{\phi}) & \cos(\bar{\phi}) & \cos(\bar{\theta})\sin(\bar{\phi}) \\ \cos(\bar{\theta}) & 0 & -\sin(\bar{\theta}) \end{bmatrix} \\ \cdot \begin{bmatrix} 1 & 0 & 0 \\ 0 & \cos(\alpha) & -\sin(\alpha) \\ 0 & \sin(\alpha) & \cos(\alpha) \end{bmatrix}. \tag{10}$$

In (10), $\bar{\phi}$ and $\bar{\theta}$ coincide with respectively the azimuth and the elevation of the nominal direction. The angle α describes how the pdf is tilted on $\mathbb{S}_2$. A detailed description of the meanings of $\boldsymbol{\gamma}_1$, $\boldsymbol{\gamma}_2$ and $\boldsymbol{\gamma}_3$ can be found in [6]. Note that when η equals 0, the FB$_5$ pdf does not depend on the values of α and the equal-value contours of $f_{\mathrm{FB}_5}(\boldsymbol{\Omega})$ are circles. For $\eta \in (0, 1/2)$, the equal-density contours of the pdf exhibit the ovalness, which becomes significant as η increases. The equal-value contours resemble ellipses when κ is small. Fig. 1 depicts the FB$_5$ pdf for the parameter setting reported in the caption of this figure.

The parameters of $f_d(\boldsymbol{\Omega})$ are concatenated in the vector $\tilde{\boldsymbol{\theta}}_d \doteq [\bar{\phi}_d, \bar{\theta}_d, \kappa_d, \eta_d, \alpha_d]$. We use a vector $\boldsymbol{\theta}$ to represent all unknown model parameters in (1), i.e.

$$\boldsymbol{\theta} \doteq [P_1, P_2, \ldots, P_D, \tilde{\boldsymbol{\theta}}_1, \tilde{\boldsymbol{\theta}}_2, \ldots, \tilde{\boldsymbol{\theta}}_D]. \tag{11}$$
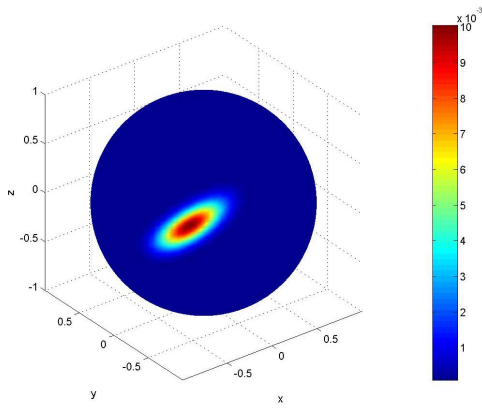
Figure 1. The FB$_5$ pdf with $\bar{\phi} = 135°, \bar{\theta} = 18°, \alpha = 144°, \kappa = 80$ and $\eta = 0.375$. The color bar to the right of the plot shows the magnitude expressed in linear scale.

III. ESTIMATION OF THE MODEL PARAMETERS

In a scenario with multiple path components, as depicted by (1), the problem at hand is to estimate the parameter vector $\boldsymbol{\theta}$. Maximum likelihood estimation of $\boldsymbol{\theta}$ requires to solve a $6D$ dimensional non-linear optimization problem. The high computational complexity involved prohibits the implementation of the maximum likelihood estimation in practise. In the sequel, we derive a SAGE algorithm [7] as an approximation of the maximum likelihood estimator of $\boldsymbol{\theta}$.

A. Admissible hidden data

We choose the subsets of parameters updated at the different iterations of the SAGE algorithm to be the sets including the parameters characterizing individual path components. Hence, in Iteration $i = 1, 2, \ldots$, the parameter subset $\boldsymbol{\theta}_d \doteq [P_d, \tilde{\boldsymbol{\theta}}_d]$ with $d = [(i-1) \mod D] + 1$ is updated.

We define the admissible hidden data associated with $\boldsymbol{\theta}_d$ as

$$\boldsymbol{X}_d(t) \doteq \boldsymbol{H}_d(t)u(t) + \boldsymbol{W}(t)$$
$$= \left[\int_{\mathbb{S}_2} \boldsymbol{c}(\boldsymbol{\Omega})h_d(t;\boldsymbol{\Omega})\mathrm{d}\boldsymbol{\Omega}\right]u(t) + \boldsymbol{W}(t). \quad (12)$$

It follows from the properties of $h_d(t;\boldsymbol{\Omega})$ that $\boldsymbol{H}_d(t)$ is constant within individual observation intervals, i.e.

$$\boldsymbol{H}_d(t) \doteq \boldsymbol{H}_{d,n} = \int_{\mathbb{S}_2} \boldsymbol{c}(\boldsymbol{\Omega})h_{d,n}(\boldsymbol{\Omega})\mathrm{d}\boldsymbol{\Omega}. \quad (13)$$

The output of a correlator

$$\tilde{\boldsymbol{H}}_{d,n} \doteq \int_{t_n}^{t_n+T} \boldsymbol{x}_d(t)u(t)^*\mathrm{d}t, \quad n = 1, \ldots, N \quad (14)$$

when the input is the observation $\boldsymbol{X}_d(t) = \boldsymbol{x}_d(t)$ can be written as

$$\tilde{\boldsymbol{H}}_{d,n} = \boldsymbol{H}_{d,n} + \boldsymbol{N}_n, \quad (15)$$

where $\boldsymbol{N}_n \in \mathbb{C}^M$, $n = 1, \ldots, N$ is a sequence of N independent random vectors, the entries of which are independent circularly symmetric Gaussian random variables with variance σ_w^2. Invoking the central limit theorem, the elements of $\tilde{\boldsymbol{H}}_{d,n}$ in (12) are assumed to be Gaussian random variables. The vectors $\tilde{\boldsymbol{H}}_{d,1}, \ldots, \tilde{\boldsymbol{H}}_{d,N}$ form a sufficient statistic for the estimation of $\boldsymbol{\theta}_d$.

B. Expectation Step

In the Expectation (E-) step of Iteration i, we compute the expectation of the likelihood of $\boldsymbol{\theta}_d$ conditioned on the observation $\boldsymbol{Y}(t) = \boldsymbol{y}(t)$ and assuming that $\boldsymbol{\theta} = \widehat{\boldsymbol{\theta}}^{[i-1]}$:

$$Q(\boldsymbol{\theta}_d|\widehat{\boldsymbol{\theta}}^{[i-1]}) \doteq \mathrm{E}\left[\Lambda(\boldsymbol{\Omega}_d; \boldsymbol{x}_d)|\boldsymbol{Y}(t) = \boldsymbol{y}(t), \widehat{\boldsymbol{\theta}}^{[i-1]}\right]. \quad (16)$$

Here, $\widehat{\boldsymbol{\theta}}^{[i-1]}$ denotes the parameter estimates obtained in the $(i-1)$th iteration and $\Lambda(\boldsymbol{\Omega}_d; \boldsymbol{x}_d)$ represents the log-likelihood function of $\boldsymbol{\Omega}_d$ given an observation $\boldsymbol{X}_d(t) = \boldsymbol{x}_d(t)$. It can be shown that (16) is of the form

$$Q(\boldsymbol{\theta}_d|\widehat{\boldsymbol{\theta}}^{[i-1]}) = -\ln|\boldsymbol{\Sigma}_{\tilde{\boldsymbol{H}}_d}(\boldsymbol{\theta}_d)|$$
$$- \mathrm{tr}\left[(\boldsymbol{\Sigma}_{\tilde{\boldsymbol{H}}_d}(\boldsymbol{\theta}_d))^{-1} \cdot \widehat{\boldsymbol{\Sigma}}_{\tilde{\boldsymbol{H}}_d}(\widehat{\boldsymbol{\theta}}^{[i-1]})\right], \quad (17)$$

where $\mathrm{tr}[\cdot]$ is the trace of the matrix given as an argument and $\boldsymbol{\Sigma}_{\tilde{\boldsymbol{H}}_d}(\boldsymbol{\theta}_d)$ is the covariance matrix of $\tilde{\boldsymbol{H}}_{d,n}$:

$$\boldsymbol{\Sigma}_{\tilde{\boldsymbol{H}}_d}(\boldsymbol{\theta}_d) = P_d \int_{\mathbb{S}_2} \boldsymbol{c}(\boldsymbol{\Omega})\boldsymbol{c}(\boldsymbol{\Omega})^{\mathrm{H}}f_d(\boldsymbol{\Omega})\mathrm{d}\boldsymbol{\Omega} + \sigma_w^2\boldsymbol{I}_M \quad (18)$$

with $[\cdot]^{\mathrm{H}}$ denoting the Hermitian operator. In (17), $\widehat{\boldsymbol{\Sigma}}_{\tilde{\boldsymbol{H}}_d}(\boldsymbol{\theta})$ is the conditional covariance matrix of $\tilde{\boldsymbol{H}}_{d,n}$ given the observation $\boldsymbol{y}(t)$ for $\boldsymbol{\theta}$. It can be shown that $\widehat{\boldsymbol{\Sigma}}_{\tilde{\boldsymbol{H}}_d}(\widehat{\boldsymbol{\theta}}^{[i]})$ is calculated as (19), where

$$\boldsymbol{\Sigma}_{\tilde{\boldsymbol{H}}}(\widehat{\boldsymbol{\theta}}^{[i]}) = \sum_{d=1}^{D} \boldsymbol{\Sigma}_{\tilde{\boldsymbol{H}}_d}(\widehat{\boldsymbol{\theta}}_d^{[i]}) + \sigma_w^2\boldsymbol{I}_M, \quad (20)$$

and

$$\widehat{\boldsymbol{\Sigma}}_{\tilde{\boldsymbol{H}}} = \frac{1}{N}\sum_{n=1}^{N} \tilde{\boldsymbol{H}}_n\tilde{\boldsymbol{H}}_n^{\mathrm{H}} \quad (21)$$

with $\tilde{\boldsymbol{H}}_n \doteq \int_{t_n}^{t_n+T} \boldsymbol{y}(t)u(t)^*\mathrm{d}t$, $n = 1, \ldots, N$.

C. Maximization Step

In the M-step, the estimate $\widehat{\boldsymbol{\theta}}_d^{[i]}$ is calculated as

$$\widehat{\boldsymbol{\theta}}_d^{[i]} = \arg\max_{\boldsymbol{\theta}_d} Q(\boldsymbol{\theta}_d|\widehat{\boldsymbol{\theta}}^{[i-1]}). \quad (22)$$

By applying a coordinate-wise updating procedure similar to the one used in [8], the required multiple-dimensional maximization can be reduced to multiple one-dimensional maximization problems. This coordinate-wise updating still remains within the SAGE framework with the admissible data given in (12).

$$\widehat{\boldsymbol{\Sigma}}_{\tilde{\boldsymbol{H}}_d}(\widehat{\boldsymbol{\theta}}^{[i]}) = \boldsymbol{\Sigma}_{\tilde{\boldsymbol{H}}_d}(\widehat{\boldsymbol{\theta}}_d^{[i]}) + \boldsymbol{\Sigma}_{\tilde{\boldsymbol{H}}_d}(\widehat{\boldsymbol{\theta}}_d^{[i]})\left[\boldsymbol{\Sigma}_{\tilde{\boldsymbol{H}}}(\widehat{\boldsymbol{\theta}}^{[i]})\right]^{-1}(\widehat{\boldsymbol{\Sigma}}_{\tilde{\boldsymbol{H}}} - \boldsymbol{\Sigma}_{\tilde{\boldsymbol{H}}_d}(\widehat{\boldsymbol{\theta}}_d^{[i]})) \cdot \left[\boldsymbol{\Sigma}_{\tilde{\boldsymbol{H}}}(\widehat{\boldsymbol{\theta}}^{[i]})\right]^{-1}\boldsymbol{\Sigma}_{\tilde{\boldsymbol{H}}_d}(\widehat{\boldsymbol{\theta}}_d^{[i]}), \quad (19)$$

(a) Surroundings of the Tx. (b) Surroundings of the Rx.

(c) Map of the premises.
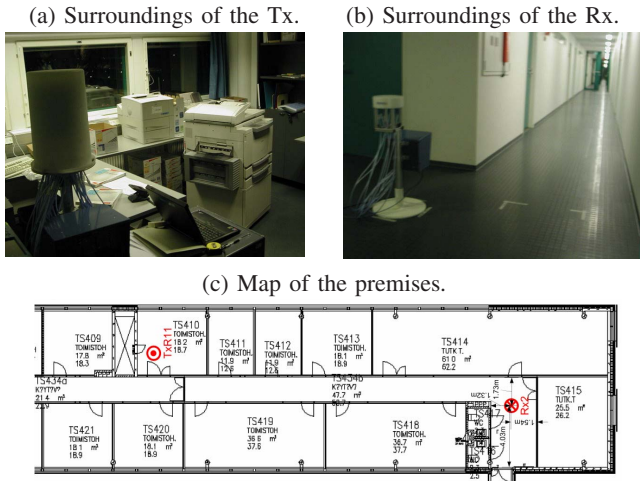
Figure 2. Photographs and map of the premises where the measurement experiment was conducted.

d	$\bar{\phi}_d$ [°]	$\hat{\bar{\theta}}_d$ [°]	$\hat{\kappa}_d$	$\hat{\eta}_d$	$\hat{\alpha}_d$ [°]	$\hat{P}_d[10^{-10}]$	$\hat{P}_d/\hat{P}_1$ [dB]
1	−84	4	140	0.33	59.3	7.10	0
2	114	−4	160	0.49	15.8	5.72	−1
3	44	−10	923	0.00	26.5	5.19	−1
4	−24	8	923	0.17	144.0	4.10	−2

D. Initialization Step

In the initialization step, the nominal AoAs and EoAs of the path components are estimated using a SAGE algorithm derived based on the specular-path model [8]. The parameters which cannot be estimated using this method are set equal certain predefined values. More specifically, the estimates of the concentration parameters κ_d, $d = 1, \ldots, D$ are set equal to 100 and the ovalness parameters are set equal to zero. With this setting it is assumed a priori that the path components are close to specular path components. This initialization procedure has proved to work well for measurement data in the experimental scenarios in which it was tested.

IV. EXPERIMENTAL INVESTIGATIONS

The measurement data were collected using the Elektrobit Propsound CS switched channel sounder [2] in an office building. The sounder was used in a MISO (multiple-input single-output) configuration where the Rx has a single antenna and the Tx is equipped with a 50-element omnidirectional antenna array. A detailed description of the sounder, the array and the measurement settings can be found in [2]. During the measurement, the Rx was located in a corridor and the Tx was placed in an office room. Two photographs and the map shown in Fig. 2 depict the surroundings of the Rx and Tx. The locations of the Tx and the Rx are marked with the symbols $\odot$ and $\otimes$ respectively on the map. During the measurement period, both Tx and Rx were fixed. People were moving in the office where the Tx was located. These movements created the randomness of the radio channel. Due to this fact, the uncorrelated scattering condition as depicted in (7) is considered to be valid.

The data obtained from 50 consecutive measurement cycles covering a period of 3.3 seconds are considered. A measurement cycle is referred to as the interval within which all 50 subchannels are sounded once. In this preliminary study, we investigate dispersion of individual path components in direction of departure and neglect dispersion in other dimensions. To this aim, we consider the output of the Rx antenna within the relative delay bin 160-170 ns. The narrow-band signal model (1) is applicable in the considered scenario for this delay bin. The parameter estimators derived based on the SAGE algorithm can be easily modified to estimate the parameters of the DoD psdfs of individual path components.

The SAGE algorithm is applied while assuming that the number of the path components is known and equals 4 in the considered scenario. Totally 10 SAGE iteration cycles are performed. Here, an iteration cycle is referred to as the procedure in which the estimates of all elements in $\boldsymbol{\theta}$ are updated once. In the M-step we select the quantization step to coincide with the resolution of the calibration measurements, i.e. be $2°$ in both azimuth and elevation.

Fig. 3 depicts the estimation results returned by the SAGE algorithm. The parameter estimates are reported in Table I. The notation $\mathrm{Bartlett}(\cdot)$ arising in the captions of Fig. 3(a) and Fig. 3(b) denotes the power spectrum estimate obtained with Bartlett beamformer [9] using the covariance matrix given as an argument. Fig. 3(c) demonstrates the azimuth-elevation psdf corresponding to the estimate of the direction psdf $\hat{P}(\boldsymbol{\Omega})$ of the radio channel. It can be observed that the azimuth-elevation psdfs of individual path components estimated using the SAGE algorithm are noticeably more concentrated than the corresponding footprints visible in $\mathrm{Bartlett}(\boldsymbol{\Sigma}_{\tilde{H}}(\hat{\boldsymbol{\theta}}))$. These psdfs differ in concentration, ovalness and tilt angle. The "blurring" effect arising in the Bartlett spectrum is due to the response of the Rx array.

The footprints of the path components shown in $\mathrm{Bartlett}(\boldsymbol{\Sigma}_{\tilde{H}}(\hat{\boldsymbol{\theta}}))$ and $\mathrm{Bartlett}(\hat{\boldsymbol{\Sigma}}_{\tilde{H}})$ are observed to be similar. This implies that the reconstructed covariance matrix computed using the parameter estimates is close to the sample covariance matrix. We also observe some differences in the shapes and the (local) maxima of the corresponding footprints. These differences are supposed to be caused by discrepancies between the "true" normalized psdfs of individual path components and the FB_5 pdf. Another possible reason for the difference is that dispersion in other dimensions, e.g. in delay, is not considered.

V. CONCLUSIONS

In this contribution, we derived a SAGE algorithm for estimation of the parameters characterizing the direction power spectral density function (psdf) of individual path components in a radio propagation channel. The Fisher-Bingham-
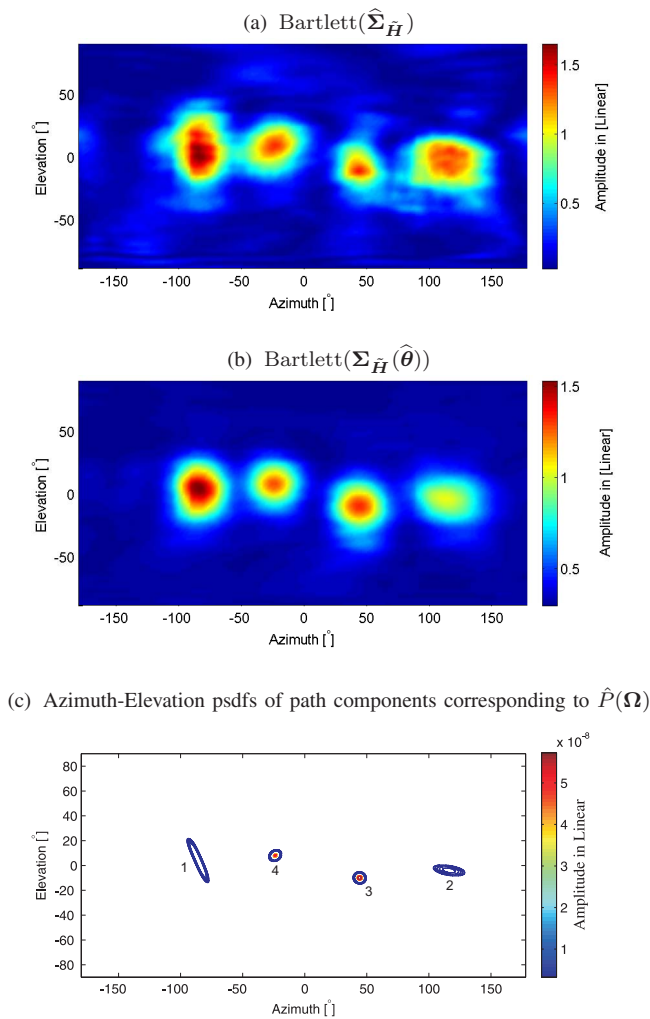
(a) $\mathrm{Bartlett}(\widehat{\boldsymbol{\Sigma}}_{\tilde{H}})$

(b) $\mathrm{Bartlett}(\boldsymbol{\Sigma}_{\tilde{H}}(\widehat{\boldsymbol{\theta}}))$

(c) Azimuth-Elevation psdfs of path components corresponding to $\hat{P}(\boldsymbol{\Omega})$

Figure 3. Estimates of the azimuth-elevation psdf within the delay bin 160-170 ns. The estimates of the parameters are shown in Table I. The indices of the path components reported in Table I are consistent with those given in Figure 3(c).

path parameters with large probabilities of occurrence.

VI. ACKNOWLEDGEMENT

The authors would like to acknowledge Elektrobit Corp., Finland, for providing the data and also Nicolai Czink for doing the measurements.

REFERENCES

[1] C. B. Ribeiro, A. Richter, and V. Koivunen, "Stochastic maximum likelihood estimation of angle- and delay-domain propagation parameters," in *Proceedings of the 16th IEEE International Symposium on Personal, Indoor and Mobile Radio Communications (PIMRC)*, vol. 1, Berlin, Germany, 2005, pp. 624 – 628.

[2] X. Yin, T. Pedersen, N. Czink, and B. H. Fleury, "Parametric characterization and estimation of bi-azimuth dispersion of path components," in *Proceedings of the 7th IEEE International Workshop on Signal Processing Advances for Wireless Communications (SPAWC)*, Nice, France, July 2006.

[3] X. Yin, L. Liu, D. Nielsen, N. Czink, and B. H. Fleury, "Characterization of the azimuth-elevation power spectrum of individual path components," in *Proceedings of the International ITG/IEEE Workshop on Smart Antennas (WSA)*, Vienna, Austria, Feb. 2007.

[4] X. Yin, T. Pedersen, N. Czink, and B. H. Fleury, "Parametric characterization and estimation of bi-azimuth and delay dispersion of path components," in *Proceedings of The First European Conference on Antennas and Progation (EuCAP)*, Acropolis, Nice, France, November 2006.

[5] B. H. Fleury, "First- and second-order characterization of direction dispersion and space selectivity in the radio channel," *IEEE Trans. Information Theory*, no. 6, pp. 2027–2044, Sept. 2000.

[6] J. T. Kent, "The Fisher-Bingham distribution on the sphere," *Journal of the Royal Statistical Society, Serieal B (Methodological)*, vol. 44, pp. 71–80, 1982.

[7] J. A. Fessler and A. O. Hero, "Space-alternating generalized expectation-maximization algorithm," *IEEE Trans. on Signal Processing*, vol. 42, no. 10, pp. 2664–2677, Oct. 1994.

[8] B. H. Fleury, M. Tschudin, R. Heddergott, D. Dahlhaus, and K. L. Pedersen, "Channel parameter estimation in mobile radio environments using the SAGE algorithm," *IEEE Journal on Selected Areas in Communications*, vol. 17, no. 3, pp. 434–450, Mar. 1999.

[9] M. Bartlett, "Smoothing periodograms from time series with continuous spectra," *Nature*, vol. 161, 1948.

[10] M. Bengtsson and B. Völcker, "On the estimation of azimuth distributions and azimuth spectra," in *Proceedings of the 54th IEEE Vehicular Technology Conference (VTC-Fall)*, vol. 3, no. 12, 2001, pp. 1612–1615.

5 probability density function (pdf) was used to describe the normalized direction psdf of individual path components. The performance of the SAGE algorithm was evaluated using measurement data. From the results we observed that the Bartlett spectrum computed with the signal covariance matrix calculated using the SAGE estimates is similar to the Bartlett spectrum computed with the sample covariance matrix. The estimated psdfs of individual path components exhibit different ovalness and tilt angle. Moreover they are more concentrated than the corresponding footprints in the Bartlett spectrum. These results indicated that dispersive path components exist in real propagation channels. In such a case, the conventional algorithms derived based on the specular-path model are inappropriate for estimation of the parameters of these path components. As shown in [10], the mismatch between the specular-path model and the "true" dispersive feature of path components results in significant errors of estimation of the